中国光学（中英文） Chinese Optics 核心期刊

Electromagnetic Bloch-like oscillations in Fibonacci metamaterial waveguide arrays

LI Zhao-hong, HAN De-zhuan

Citation:
LI Zhao-hong, HAN De-zhuan. Electromagnetic Bloch-like oscillations in Fibonacci metamaterial waveguide arrays[J]. *Chinese Optics*, 2025, 18(4): 947-953. doi: 10.37188/CO.EN-2024-0033
李召红，韩德专. 特异材料斐波那契波导阵列中的类布洛赫振荡研究[J]. 中国光学，2025，18(4)：947-953. doi: 10.37188/CO.EN-2024-0033

View online: https://doi.org/10.37188/CO.EN-2024-0033

Articles you may be interested in

Wide and narrow band switchable bi-functional metamaterial absorber based on vanadium dioxide
基于二氧化钒宽、窄带可切换的双功能超材料吸收器研究
Chinese Optics. 2022, 15(2): 387 https://doi.org/10.37188/CO.2021-0174

Bandwidth-tunable terahertz metamaterial half-wave plate component
带宽可调谐的太赫兹超构材料半波片器件
Chinese Optics. 2023, 16(3): 701 https://doi.org/10.37188/CO.2022-0198

Tunable optical metamaterials and their applications
可调谐光学超构材料及其应用
Chinese Optics. 2021, 14(4): 968 https://doi.org/10.37188/CO.2021-0080

Optical topological characteristics of two dimensional artificial metamaterials
二维人工超材料的光学拓扑性质
Chinese Optics. 2021, 14(4): 955 https://doi.org/10.37188/CO.2021-0074

Fano resonances design of metamaterials based on deep learning
基于深度学习的Fano共振超材料设计
Chinese Optics. 2023, 16(4): 816 https://doi.org/10.37188/CO.2022-0208

A vanadium dioxide-assisted switchable multifunctional metamaterial structure
二氧化钒辅助的可切换多功能超材料结构
Chinese Optics. 2023, 16(3): 514 https://doi.org/10.37188/CO.2022-0195

文章编号 2097-1842(2025)04-0947-07

Electromagnetic Bloch-like oscillations in Fibonacci metamaterial waveguide arrays

LI Zhao-hong[1*], HAN De-zhuan[2]
(1. *State Key Laboratory of Optoelectronic Materials and Technologies*, *Chongqing University of Arts and Sciences*, *Chongqing* 402160, *China*;
2. *College of Physics*, *Chongqing University*, *Chongqing* 401331, *China*)
* *Corresponding author*, *E-mail*: *at*12309@163.*com*

Abstract: This paper investigates optical transport in metamaterial waveguide arrays (MMWAs) exhibiting Bloch-like oscillations (BLOs). The MMWAs is fabricated by laterally combining metal and dielectric layers in a Fibonacci sequence. By mapping the field distribution of Gaussian wave packets in these arrays, we directly visualize the mechanical evolution in a classical wave environment. Three distinct oscillation modes are observed at different incident positions in the ninth-generation Fibonacci structure, without introducing thickness or refractive index gradient in any layer. Additionally, the propagation period of BLOs increases with a redshift of the incident wavelength for both ninth- and tenth-generation Fibonacci MMWAs. These findings provide a valuable method for manipulating BLOs and offer new insights into optical transport in metamaterials, with potential applications in optical device and wave control technologies.

Key words: quasiperiodic; Bloch-like oscillation; metamaterial; Fibonacci

特异材料斐波那契波导阵列中的类布洛赫振荡研究

李召红[1*], 韩德专[2]
(1. 重庆文理学院 光电子材料与技术研究所, 重庆 402160;
2. 重庆大学 物理学院, 重庆 401331)

摘要: 本文研究了一种特异材料构成的波导阵列中光传输的类布洛赫振荡特性。这种准周期波导阵列由金属和介质两种介质按斐波那契数列的顺序排列组成。通过研究高斯脉冲在结构中传输时的光场分布, 可以直观地观察其光场演化情况。在没有引入厚度梯度或介电常数梯度的情形下, 在第九代斐波那契准周期波导中发现了 3 种振荡模式。另外, 随着入射脉冲波长的增加, 在第九代和第十代斐波那契准周期波导中类布洛赫振荡周期产生了红移, 这为布洛赫振荡调控提供了一种有意义的途径。

收稿日期: 2024-10-24; **修订日期:** 2024-11-14

基金项目: 重庆市自然科学基金(No. cstc2019jcyj-msxmX0238); 重庆市教委科学技术研究项目(No. KJQN201901301); 重庆市博士后研究资助项目

Supported by the Natural Science Foundation of Chongqing (No. cstc2019jcyj-msxmX0238); The Youth Fund Project of the Science and Technology Research Programme of the Chongqing Education Commission (No. KJQN201901301); Postdoctoral Research Fellowship from Chongqing

关 键 词：准周期材料；布洛赫振荡；特异材料；斐波那契
中图分类号：O438 文献标志码：A doi：10.37188/CO.EN-2024-0033 CSTR：32171.14.CO.EN-2024-0033

1 Introduction

The well-known Bloch oscillation (BO) was first predicted in 1929 for a periodic potential excited by an external homogeneous static electric field[1]. As a classical prediction, BO remained an elusive phenomenon for over six decades due to rapid decoherence in electronic systems. This fundamental problem was finally resolved with the groundbreaking experimental observation of BOs in semiconductor superlattices by Feldmann *et al*.[2]. Since then, superlattices in waveguide arrays have emerged as an ideal platform for observing both linear and nonlinear optical Bloch oscillations[3]. In recent years, abundant novel phenomena related to imaging polarimetry have been observed in various systems, including optical analog processing[4], metalens imaging polarimetry[5], and angular spectrum differentiation[6]. To date, BOs have been extensively investigated in a wide range of optical sub-micron and nanoscale optical systems, such as coupled optical waveguides[7-12], period-doubling topological systems[13], Floquet-Bloch oscillations[14], acoustic superlattices[15-16] and quantum particles in periodic media under the influence of a constant external force[17]. Efforts are also underway to fabricate a uniform thickness metamaterial structures, such as multilayer metamaterials[18] and nanoscale optical devices[19].

Currently, significant resources are being allocated to the development of the BOs in MMWAs due to their potential for carrying optical signals via evanescent electromagnetic waves, which propagate along the interface between metal and dielectric layers in various dispersive systems[20-24]. For instance, BOs have been realized in three-dimensional waveguide arrays by introducing a refractive index gradient in dielectric layers[25] and in chirped metal-dielectric structures[26].

The recognized principle underlying optical BOs is the coupling of evanescent waves in adjacent waveguides, which results in the formation of a collective supermode. Due to the alternating total internal reflection and the transverse Bragg reflection at the boundaries, this collective supermode is confined to a specific region of the waveguide array and propagates along the longitudinal direction. To the best of our knowledge, for the general case, the realization of BOs in waveguide arrays requires either a transverse gradient in the effective refractive index or a monotonic variation in the adjacent layers. This condition is analogous to the constant electric field required for BOs of electrons in a periodic potential. Specifically, the gradient in the effective refractive index induces a variation in the propagation constant, which follows a linear relationship described by $\beta = k_0 n$, where k_0 represent the wave vector in the volume. Hence, it is evident that both the refractive index and the thickness of the layers play crucial roles in realizing BOs in periodic waveguide arrays.

Quasiperiodic systems represent an intermediate state between periodic and disordered systems, exhibiting long-range order without translational symmetry. Fibonacci is a common and representative quasiperiodic system generated through iterative rules[27-28]. Unlike the periodic system with a gradient modulation, the optical thickness of quasiperiodic systems is non-monotonic due to the absence of translational symmetry. In this paper, we aim to investigate Bloch-like Oscillations (BLOs) in a planar Fibonacci quasiperiodic MMWA. The fabrication is achieved using an ultrahigh vacuum electron beam evaporation system on a chemically cleaned glass substrate.

In this paper, we propose a planar Fibonacci waveguide array composed of silver and silicon dioxide to theoretically demonstrate spatial BLOs. Periodic oscillations are observed in the ninth- and tenth-generation Fibonacci MMWA using the exact field distributions of the incident Gaussian pulse. In

particular, we identify three distinct types of collective oscillation modes when a Gaussian pulse of the same wavelength is incident on different positions of the ninth-generation structure. The oscillation period increases with the redshift of the incident wavelength for both the ninth- and tenth-generation Fibonacci structures. Our work provides a flexible platform for implementing various interesting phenomena based on metamaterials and has potential applications in manipulating the emergence of BLOs.

2 Results and discussion

This study investigates plasmonic BLOs in MMWAs using theoretical analysis and numerical simulation techniques. The simulation models are implemented using the Finite Difference Time Domain (FDTD) method, which provided explicit and dynamic solutions. During the simulation, the Perfect Electric Conductor (PEC) layers are applied to both sides along the X-direction, and the Perfect Magnetic Conductor (PMC) layer are applied to both sides along the Z-direction, serving as numerical absorbing boundary conditions.

The quasiperiodic waveguide arrays are constructed using a Fibonacci structure composed of two types of layers: A and B. Type A consists of dielectric silicon dioxide layers, while Type B consists of metamaterial silver layers. According to the recursion formula, the ninth-generation Fibonacci quasiperiodic MMWA is configured as follows:

S_9 = ABAABABAABAABABAABABAABAABABAABAABABAABABAABAABABAABABA

The graphical representation of the ninth-generation MMWA is shown in Fig. 1. The thicknesses of layer A and layer B are $d_A = 28$ nm and $d_B = 20$ nm respectively. To simplify the analytical discussion, we ignore the dielectric dispersion and losses in the metal layer. We choose the dielectric permittivity $\varepsilon_{SiO_2} = 2.126\,6$. The real part of the permittivity for the silver in the Drude model is ε_S ($\varepsilon_S \approx 1 - \varpi_p^2/\varpi^2$) in the high frequency limit. The plasma frequency ϖ_p is that of the reference[29]. The transport property is effectively defined by the real part, while the imaginary part corresponds to the attenuation. Hence, only the effect of the real part is considered in the FDTD simulation.

The amplitude profile of a Transverse Magnetic (TM) polarized Gaussian pulse, which is normal incident along the *Y*-direction, has a specific form $H_z = \exp(-(x - x_0^2)/2\delta^2)$, where the incident position and Full Width at Half Maximum (FWHM) are x_0 and $\delta = 200$ nm, respectively. For convenience, the coordinate system's origin is set at $x_0 = 0.686$ μm, which is the center of the twenty-eighth slit dielectric layer shown in Fig. 1 (color online). The FDTD program Optiwave OptiFDTD is used to perform the simulation[30].

The trajectory of the Gaussian pulse is simulated in the quasiperiodic MMWA. It should be mentioned that the wave dispersion relation is calculated by the transfer-matrix method, since the entire Fibonacci structure can be regarded as a unit in the periodic structure[31], even the fact that the structure is the absence of translational symmetry. Thus, the pseudo-dispersion relation can be written as:

$$\cos[k_x(d_A + d_B)] = \cos(k_1 d_A)\cos(k_2 d_B) - (k_1^2\varepsilon_m^2 + k_2^2\varepsilon_a^2/2k_1k_2\varepsilon_a\varepsilon_m)\sin(k_1 d_A)\sin(k_2 d_B) \quad , \qquad (1)$$

with $k_{1,2} = \sqrt{(\varepsilon_{a,m}k_0^2 - k_z^2)}$, where k_0 is the free space wave vector, and k_x and k_z are the Bloch wave vector along the *X*-direction and the propagation constant along the *Z*-axis. In general, a simple way to obtain photonic BOs is to introduce a gradient change of the optical thickness between two adjacent waveguide layers[32]. Therefore, we first introduce a permittivity gradient α for dielectric layer, where $\alpha \in (0, 0.15)$. In general, there are 34 dielectric layers in the ninth Fibonacci quasiperiodic MMWA, and the permittivity of the *N*th layer is $\varepsilon_a = \varepsilon_0 + \alpha(N-1)$, where $N = 1, 2 \cdots 34$ and $\varepsilon_0 = 1.0$. Then, the photonic band diagram of the graded MMWA is shown in the Fig. 1(b). An inclined band

gap appears for a Gaussian pulse with wavelength ranging from 100 nm to 600 nm when the incident pulse propagates along the *X*-direction, which is well matched in Bragg mirrors, to some extent[32]. The lower index layers in the ninth Fibonacci MMWA without gradient permittivity are the equivalent to the barriers, and the lower index layers play the role of quantum wells in conventional semiconductor superlattices. Thus, the adjacent microcavities, which are the layers in the structure, are coupled to each other. And the coupling leads to the photonic Bloch-like oscillations, which are a collected supermode of the localized states with non-commensurate.

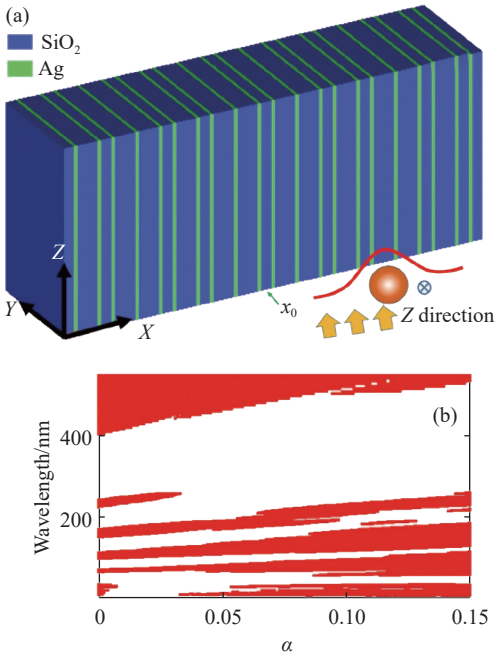

Fig. 1 (a) Schematic illustration of the 2D quasiperiodic waveguide array. The blue and green layers represent the silicon dioxide dielectric layer and the silver layer, respectively. The electromagnetic waves are incident along the *Y*-direction. The amplitude of the Gaussian pulse is shown in the red line. And the circle shows the intensity distribution. (b) The band diagram of the graded MMWA with a gradient α increasing from 0 to 0.15 for the dielectric permittivity with a relation of $\varepsilon_a = \varepsilon_0 + \alpha(N-1)$. Red regions represent the minigaps, white regions represent the minibands

The electromagnetic evolution of the pulse in the waveguide array can be simulated as shown in Fig. 2 (color online).

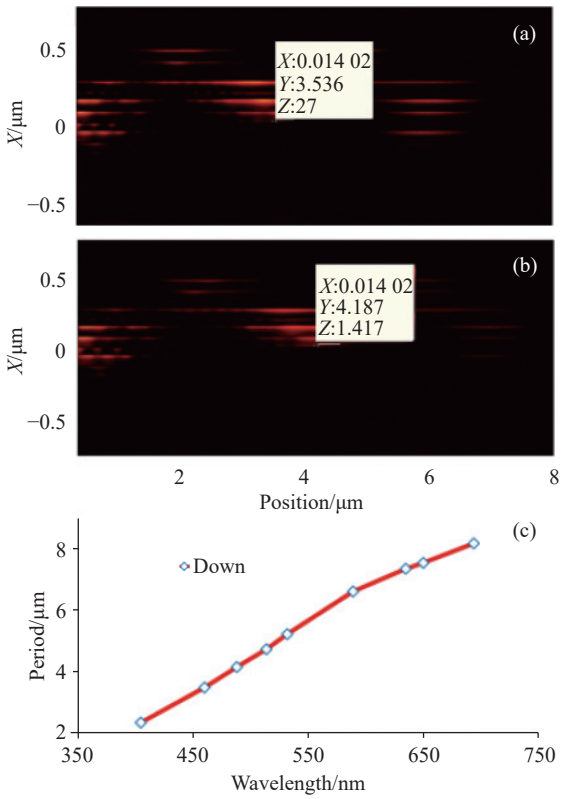

Fig. 2 (a) and (b) show contours of magnetic field intensity $|H_y|$ for Gaussian pulses with $\lambda = 460$ nm and $\lambda = 488$ nm, respectively simulated by the FDTD method. (c) The simulated period of the BLO in the waveguide arrays depends on the incident light wavelength (λ = 405, 460, 488, 514, 532, 589, 635, 650, 694 nm, respectively)

The results regarding optical BLOs are shown in Fig. 2(a), where a Gaussian pulse with FWHM $\delta = 200$ and wavelength $\lambda = 460$ nm is incident on the right side of the waveguide arrays at the position $x_0 = 0$. The simulated contour of the magnetic field $|H_y|$ for a Gaussian pulse with $\lambda = 460$ nm is shown in Fig. 2(a). It can be observed that an excited oscillating mode spreads over several waveguides and undergoes a discrete diffraction. Finally, the oscillation periods plotted in Fig. 2(b) are about 3.54 μm and 4.19 μm, respectively, while the corresponding oscillation amplitudes have approximately the same value of 0.5 μm. In view of the fact that, quasiperiodic incommensurate MMWA deals with inhomogeneous refractive index, that the maximum value of the dielectric constant is 2.13 in the region below the position x_0, while the permittivity of silver is approximately −11.54. We associate the local-

ization of the electromagnetic field with the layers adjacent to the quasiperiodic structure, which have similarities to the electronic field influenced by a non-uniform force in a non-periodic potential.

When the Gaussian pulse impinges on the positions $x = 0.34$, $x = 0$ and $x = -0.34$, respectively, the distribution of magnetic field intensity is shown in Fig. 3 (color online).

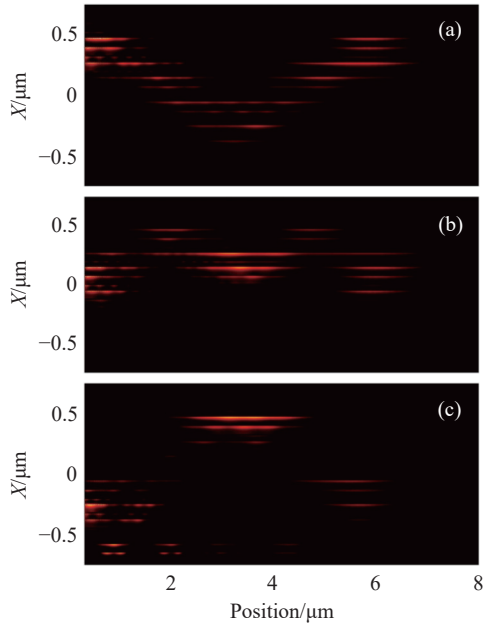

Fig. 3　Contours of magnetic field intensity $|H_y|$ for a Gaussian pulse impinging on the positions $x = 0.34$, $x = 0$ and $x = -0.34$

By comparing the Fig. 3(a)−3(c), we can identify some remarkable features. Firstly, there are three different types of collective oscillation modes in which the electromagnetic field is initially inclined to oscillate in the positive and negative directions along the *X*-axis. The oscillating direction depends on the incident position. For $x_0 = 0.314$, the excited mode oscillates along the negative direction of the *X*-axis. Conversely, for $x = 0$ and $x = -0.34$, the excited mode oscillates along the positive direction of the *X*-axis and some of the electromagnetic field also spills out in the reverse direction. Secondly, there are slight distinctions between the periods of each oscillating mode corresponding to 5.92 μm, 6.04 μm and 5.85 μm from Fig. 3(a) to Fig. 3(c). Lastly, the pattern of the magnetic field distribution differs significantly, with a noticeable increase in the field energy leakage around $x = -0.5$ in Fig. 3(c) due to tunneling between the neighboring layers.

Fig. 4 shows the simulated results of the magnetic field evolution within the ninth-generation Fibonacci quasiperiodic waveguide arrays for the Gaussian pulse impinging on the fixed position $x = 0.21$. The incident wavelengths of the Gaussian pulse are 488 nm, 514 nm and 532 nm, respectively. According to the above analyses, the coordinates of the trough for the oscillation shift gradually from $z = 3.85$ to $z = 4.92$, while the distribution of the magnetic field is mainly confined to the area between $x = 0.48$ and $x = -0.22$.

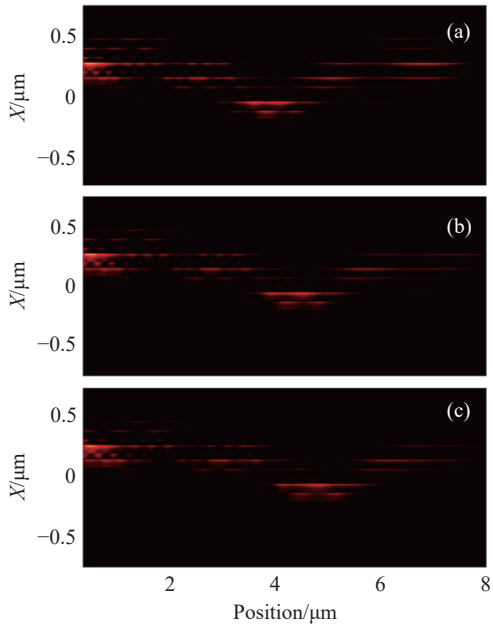

Fig. 4　(a)−(c) Contours of magnetic field intensity $|H_y|$ for Gaussian pulse impinging on the position of $x = 0.21$

Additionally, in another general scenario, several different Gaussian pulses are selected to impinge on the tenth generation Fibonacci MEWA. The field distributions with the same pattern which are the Bloch-like oscillations are shown in Figs. 5(a)−(c). The input port of the Gaussian pulse is $x = 0.34$. From Figs. 5(a)−5(c), it can be observed that all the oscillations initially start with along the positive direction of the X-axis. The periods of oscillation for the input wavelengths of λ= 488 nm, 514 nm, 532 nm are 4.89 μm, 5.56 μm,

5.89 μm, respectively. This observation also confirms a redshift, consistent with the one found in the ninth-generation Fibonacci MEWA.

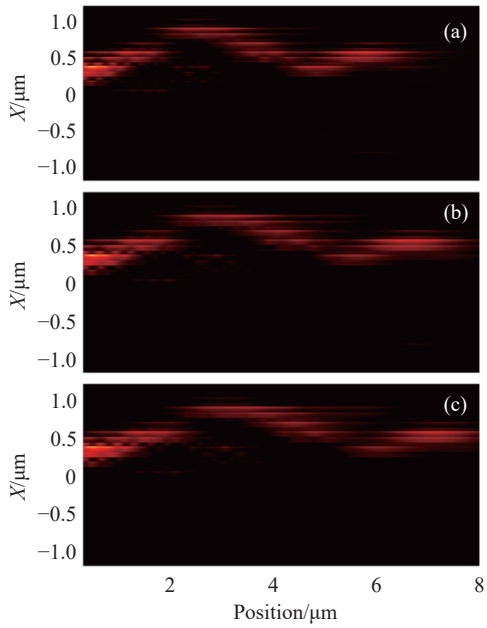

Fig. 5 (a)–(c) Contours of magnetic field intensity $|H_y|$ for Gaussian pulse impinging on the position of $x = 0.34$ in the tenth Fibonacci waveguide arrays

3 Conclusion

In summary, we have investigated spatial BLOs in the ninth- and tenth-generation Fibonacci planar quasiperiodic waveguide arrays using FDTD simulations. Three distinct collective oscillation modes were observed in the ninth-generation quasiperiodic structure based on the evolution of the electromagnetic field. Additionally, we found that the oscillation period increases with the redshift of the incident wavelength for both Fibonacci structures. The non-monotonic optical thickness also influences BLOs, which are distinctly different from those observed in periodic structures. As a result, the findings presented in this paper provide a flexible platform for implementing a variety of interesting phenomena related to metamaterials and may have potential applications in manipulating the emergence of BLOs.

References:

[1] BLOCH F. Über die quantenmechanik der elektronen in kristallgittern[J]. *Zeitschrift für Physik*, 1929, 52(7): 555-600.

[2] FELDMANN J, LEO K, SHAH J, *et al*.. Optical investigation of Bloch oscillations in a semiconductor superlattice[J]. *Physical Review B*, 1992, 46(11): 7252-7255.

[3] MORANDOTTI R, PESCHEL U, AITCHISON J S, *et al*.. Experimental observation of linear and nonlinear optical bloch oscillations[J]. *Physical Review Letters*, 1999, 83(23): 4756-4759.

[4] DENG M, COTRUFO M, WANG J, *et al*.. Broadband angular spectrum differentiation using dielectric metasurfaces[J]. *Nature Communications*, 2024, 15(1): 2237.

[5] HUANG ZH R, ZHENG Y Q, LI J H, *et al*.. High-resolution metalens imaging polarimetry[J]. *Nano Letters*, 2023, 23(23): 10991-10997.

[6] BERND K, MAXIM E. Angular bloch oscillations and their applications[J]. *Quantum Science and Technology*, 2025, 10(1): 015025.

[7] LENZ G, TALANINA I, DE STERKE C M. Bloch oscillations in an array of curved optical waveguides[J]. *Physical Review Letters*, 1999, 83(5): 963-966.

[8] BREID B M, WITTHAUT D, KORSCH H J. Bloch-Zener oscillations[J]. *New Journal of Physics*, 2006, 8: 110.

[9] BLOCK A, ETRICH C, LIMBOECK T, *et al*.. Bloch oscillations in plasmonic waveguide arrays[J]. *Nature Communications*, 2014, 5(1): 3483.

[10] WETTER H, FEDOROVA Z, LINDEN S. Observation of the Wannier–Stark ladder in plasmonic waveguide arrays[J]. *Optics Letters*, 2022, 47(12): 3091-3094.

[11] ZHAO Y, CHEN Y, HOU ZH SH, *et al*.. Polarization-dependent Bloch oscillations in optical waveguides[J]. *Optics Letters*, 2022, 47(3): 617-620.

[12] LI J H, HU G W, SHI L N, *et al*.. Full-color enhanced second harmonic generation using rainbow trapping in ultrathin hyperbolic metamaterials[J]. *Nature Communications*, 2021, 12(1): 6425.

[13] KHAN N, WANG P, FU Q D, *et al*.. Observation of period-doubling Bloch oscillations[J]. *Physical Review Letters*,

2024, 132(5): 053801.

[14] ZHANG ZH, LI Y, CHEN CH H, *et al*.. Polychromatic photonic Floquet-Bloch oscillations[J]. *Optics Express*, 2024, 32(6): 10703-10714.

[15] SANCHIS-ALEPUZ H, KOSEVICH Y A, SÁNCHEZ-DEHESA J. Acoustic analogue of electronic Bloch oscillations and resonant Zener tunneling in ultrasonic superlattices[J]. *Physical Review Letters*, 2007, 98(13): 134301.

[16] NATALE G, BLAND T, GSCHWENDTNER S, *et al*.. Bloch oscillations and matter-wave localization of a dipolar quantum gas in a one-dimensional lattice[J]. *Communications Physics*, 2022, 5(1): 227.

[17] ZHANG W X, YUAN H, WANG H T, *et al*.. Observation of Bloch oscillations dominated by effective anyonic particle statistics[J]. *Nature Communications*, 2022, 13(1): 2392.

[18] PRADHAN S K, XIAO B, SKUZA J R, *et al*.. Effects of dielectric thickness on optical behavior and tunability of one-dimensional Ag/SiO_2 multilayered metamaterials[J]. *Optics Express*, 2014, 22(10): 12486-12498.

[19] MAIER S A, BRONGERSMA M L, KIK P G, *et al*.. Plasmonics—a route to nanoscale optical devices[J]. *Advanced Materials*, 2001, 13(19): 1501-1505.

[20] ZHANG J X, ZHANG L D, XU W. Surface plasmon polaritons: physics and applications[J]. *Journal of Physics D: Applied Physics*, 2012, 45(11): 113001.

[21] OZBAY E. Plasmonics: merging photonics and electronics at nanoscale dimensions[J]. *Science*, 2006, 311(5758): 189-193.

[22] ZHOU Y, LIU Q, WANG CH K, *et al*.. Trapping effect and trajectory control of surface plasmon polaritons in a metal-dielectric-metal waveguide[J]. *Physical Review A*, 2020, 102(6): 063516.

[23] LIN W H, CHEN Y F, WANG W J. Array periodical nanofocusing effect in nanoscale three-dimensional surface plasmon polariton waveguide arrays[J]. *Journal of the Optical Society of America B*, 2020, 37(3): 762-766.

[24] LIN W H, WANG W J. The spatial plasmonic Bloch oscillations in nanoscale three-dimensional surface plasmon polaritons metal waveguide arrays[J]. *Optics Express*, 2019, 27(17): 24591-24600.

[25] DAVOYAN A R, SHADRIVOV I V, SUKHORUKOV A A, *et al*.. Plasmonic Bloch oscillations in chirped metal-dielectric structures[J]. *Applied Physics Letters*, 2009, 94(16): 161105.

[26] MEDINA-MAGALLÓN J E, PÉREZ-AGUILAR H, ZHEVANDROV-BOLSHAKOVA P, *et al*.. Excitation of surface plasmon polaritons in photonic crystal waveguides that involve dispersive metamaterial[J]. *Journal of Physics: Conference Series*, 2019, 1221: 012010.

[27] LI ZH H, PANG X N, DONG J W, *et al*.. Electromagnetic Bloch-like oscillations in one-dimensional quasicrystal consisting of negative permeability metamaterial[J]. *Europhysics Letters*, 2011, 95(3): 36004.

[28] VASCONCELOS M S, ALBUQUERQUE E L. Plasmon-polariton fractal spectra in quasiperiodic multilayers[J]. *Physical Review B*, 1998, 57(5): 2826-2833.

[29] RAETHER H. Surface plasmons on smooth surfaces[M]//RAETHER H. Surface Plasmons on Smooth and Rough Surfaces and on Gratings. Berlin, Heidelberg: Springer, 1988: 4-39.

[30] LOURENÇO P, FANTONI A, FERNANDES M, *et al*.. FDTD analysis of Aluminum/a-Si: H surface plasmon waveguides[J]. *Proceedings of SPIE*, 2018, 10526: 105262D.

[31] VERSLEGERS L, CATRYSSE P B, YU Z F, *et al*.. Deep-subwavelength focusing and steering of light in an aperiodic metallic waveguide array[J]. *Physical Review Letters*, 2009, 103(3): 033902.

[32] MALPUECH G, KAVOKIN A, PANZARINI G, *et al*.. Theory of photon Bloch oscillations in photonic crystals[J]. *Physical Review B*, 2001, 63(3): 035108.

Author Biographics:

LI Zhao-hong (1983—), male, born in Jining City, Shandong Province, Associate Professor, received his Ph.D. from Sun Yat-sen University in 2012. He is mainly engaged in the research of the interaction of light with optical structures. E-mail: at12309@163.com